Published in final edited form as:
Biomaterials. 2009 October ; 30(30): 6006–6016. doi:10.1016/j.biomaterials.2009.07.015.

A self-assembling nanoparticle for paclitaxel delivery in ovarian cancer

Kai Xiao[a,b], **Juntao Luo**[a,*], **Wiley Fowler**[c], **Yuanpei Li**[a,d], **Joyce Lee**[a], **Li Wang**[b], and **Kit S. Lam**[a,*]

[a]Division of Hematology & Oncology, Department of Internal Medicine, UCD Cancer Center, University of California Davis, Sacramento, CA 95817, USA

[b]National Chengdu Center for Safety Evaluation of Drugs, West China Hospital, Sichuan University, Chengdu, 610041, China

[c]Division of Gynecologic Oncology, Department of Obstetrics and Gynecology, UCD Cancer Center, University of California Davis, Sacramento, CA 95817, USA

[d]The First Affiliated Hospital, Sun Yat-Sen University, GuangZhou, 510080, China

Abstract

Paclitaxel (PTX) is one of the most effective chemotherapeutic drugs for the treatment of a variety of cancers. However, it is associated with serious side effects caused by PTX itself and the Cremophor EL emulsifier. In the present study, we report the development of a well-defined amphiphilic linear–dendritic copolymer (named as telodendrimer) composed of polyethylene glycol (PEG), cholic acid (CA, a facial amphiphilic molecule) and lysine, which can form drug-loaded core/shell micelles when mixed with hydrophobic drug, such as PTX, under aqueous condition. We have used PEG^{5k}-CA_8, a representive telodendrimer, to prepare paclitaxel-loaded nanoparticles (PTX-PEG^{5k}-CA_8 NPs) with high loading capacity (7.3 mg PTX/mL) and a size of 20–60 nm. This novel nanoformulation of PTX was found to exhibit similar *in vitro* cytotoxic activity against ovarian cancer cells as the free drug (Taxol®) or paclitaxel/ human serum albumin nanoaggregate (Abraxane®). The maximum tolerated doses (MTDs) of PTX-PEG^{5k}-CA_8 NPs after single dose and five consective daily doses in mice were approximately 75 and 45 mg PTX/kg, respectively, which were 2.5-fold higher than those of Taxol®. In both subcutaneous and orthotopic intraperitoneal murine models of ovarian cancer, PTX-PEG^{5k}-CA_8 NPs achieved superior toxicity profiles and antitumor effects compared to Taxol® and Abraxane® at equivalent PTX doses, which were attributed to their preferential tumor accumulation, and deep penetration into tumor tissue, as confirmed by near infrared fluorescence (NIRF) imaging.

Keywords

Biocompatibility; amphiphilic linear-dendritic copolymer; micelle; drug delivery; chemotherapy; ovarian cancer

*Corresponding authors: Juntao Luo: Tel: (916)734-0905, Fax: (916)734-6415, juntao.luo@ucdmc.ucdavis.edu, Kit S. Lam: Tel: (916) 734-8012, Fax: (916)734-7946, kit.lam@ucdmc.ucdavis.edu.

1. Introduction

Ovarian cancer is the fifth leading cause of death from cancer in women and the leading cause of death from gynecological cancer in the United States. Lifetime risk of ovarian cancer is approximately 1.5%, making it the second most common gynecologic malignancy. Because these cancers tend to be relatively aggressive and there are no proven early detection tests, most patients are not diagnosed until they have reached advanced stages (III or IV) [1]. This contributes to the poor prognosis observed with ovarian cancers, with only 35% to 38% of 5-year survival rates for all stages. Standard treatment usually involves surgical staging and debulking followed by chemotherapy. Paclitaxel (PTX), which works by interfering with normal microtubule breakdown during cell division [2], is one of the first-line chemotherapeutics used for the treatment of ovarian cancer. Due to its poor solubility in water, PTX is currently formulated in a mixture of Cremophor EL/absolute ethanol (1:1 in volume) as Taxol®. However, due to the relatively large amount of Cremophor used and the nonspecific biodistribution of the drug in both tumors and normal tissues, Taxol® has been associated with serious side effects, including severe hypersensitivity reactions, myelosuppression and neurotoxicity [3,4]. PTX resistance is also seen in more than 70% of patients at the time of initial diagnosis and almost all patients upon relapse. Some mechanisms of such relapses include poor availability of systemically administered drugs and phenotypic alterations in the cancer cells [5]. Therefore, there is a tremendous incentive to develop alternative delivery system for PTX to increase its availability at tumor sites, and to maximize the therapeutic efficacy while minimizing the side effects.

With recent advances in nanotechnology, various nanomaterials, such as polymeric and metal nanoparticles, micelles, dendrimers and liposomes, are now used in pharmaceutical delivery systems for drugs such as PTX. These nanocarriers can deliver various types of drugs, and protect them from degradation and inactivation upon administration, increase the fraction of drug delivered to tumor, thereby providing a means to decrease the undesirable side effects of cytotoxic drugs [6]. As the vasculature in tumors is known to be leaky to macromolecules, and the tumor lymphatic system is also deficient, nanoparticles can preferentially accumulate in the tumor site via the enhanced permeability and retention (EPR) effects [7].

Many nanoparticles have been investigated for drug delivery, but only a few have been approved by the Food and Drug Administration (FDA) [8]. This reason may be due to their potential toxicity, poor biocompatibility, instability *in vivo*, low drug loading capacity, or batch-to-batch inconsistencies in their biophysicochemical properties. Polymeric micelles with smaller sizes (20–100 nm) have shown great promise as nanocarriers for efficient drug delivery [9–11]. Many amphiphilic block copolymers have been prepared for the delivery of paclitaxel. [12,13] The majority of them exhibited low drug loading capacity. However, the Me-PEG-b-PDLLA micelles had a very impressive PTX loading level of 25% w/w with a stability lasting for 24 hours.[14] In search for a drug nanocarrier with superior properties, we have developed a well-defined nontoxic PEG-dendritic block copolymer (refereed to as a telodendrimer) composed of polyethylene glycol (PEG), cholic acid (CA) and lysine for successful delivery of PTX in the treatment of nude mice bearing ovarian cancer xenografts. Linear-dendritic polymers are a unique class of polymers with well-defined structure and tunable aggregation properties [15,16]. Several PEG-dendritic copolymers with hydrophobic groups attached to the periphery of the dendrimer have been reported and their associated micelle formation [17–21] and drug delivery properties were studied. [22,23] Cholic acid is a natural surfactant secreted in the mammalian bile for emulsification of dietary lipids, cholesterol, and fat-soluble vitamins. It is a unique building block for the dendritic polymer construction, due to its availability, chirality, facial amphiphiles with complementary functionalities and non-toxic properties [24]. We have assembled dendritic oligomer of cholic acid to the distal end of the PEG with a series of lysine to achieve appropriate hydrophilic and hydrophobic balance. The

resulting nanocarrier has a greater PTX loading capacity (35% w/w of drug polymer ratio) and superior stability (longer than six months) compared to the PTX-loaded Me-PEG-b-PDLLA micelles (25% w/w and 24 h, respectively) reported in the literature [14]. These highly favorable pharmaceutical properties could perhaps be explained by the planar structure and the facial amphiphilicity of cholic acid and the dendritic configuration of the hydrophobic core. In addition, the hydrophilic PEG layer further stabilizes the hydrophobic aggregation in the interior of micelles and at the same time provide a "stealth" layer on the nanoparticle surface, leading to a longer circulation time of the nanoparticles following intravenous injection [25, 26].

In this study, we used PEG^{5k}-CA_8 as a representative telodendrimer comprised of an octamer of cholic acid (CA_8) linked to the terminal end of a linear 5 kDa PEG molecule (PEG^{5k}), to prepare a PTX nanoformulation for ovarian cancer treatment. The PEG^{5k}-CA_8 telodendrimer were synthesized, and incorporated PTX with or without DiD (a near infrared fluorescent (NIRF) dye) to self-assemble into micellar nanoparticles, whose morphology, size distribution, stability and drug release features were characterized. *In vitro* cytotoxicity of blank nanoparticles was assessed in normal fibroblasts, and the cell killing effects of PTX loaded PEG^{5k}-CA_8 nanoparticles (PTX-PEG^{5k}-CA_8 NPs) was tested in ovarian cancer cells. The real-time *in vivo* biodistribution and tumor targeting ability of PTX-PEG^{5k}-CA_8 NPs after intravenous or intraperitoneal injection was studied by noninvasive optical imaging technology. The anti-tumor effects and safety profiles of PTX-PEG^{5k}-CA_8 NPs were evaluated in both subcutaneous and orthotopic intraperitoneal ovarian cancer xenograft models, and compared with Taxol® and Abraxane® (Albumin-bound Paclitaxel) which were approved by FDA.

2. Materials and Methods

2.1. Materials

Paclitaxel was purchased from AK Scientific Inc. (Mountain View, CA). Monomethyl terminated polyethylene glycol mono amine (MeO-PEG-NH_2, Mw =5 kDa) was purchased from Rapp Polymere (Tübingen, Germany). (Fmoc)lysine(Fmoc)OH was purchased from NeoMPS INC (San Diego, CA, USA), Cholic acid, Cremphor EL, and MTT [3-(4, 5-dimethyldiazol-2-yl)-2, 5 diphenyl tetrazolium bromid] were purchased from Sigma-Aldrich. Hydrophobic near infrared fluorescence (NIRF) dye DiD (1,1'-dioctadecyl-3,3,3',3'-tetramethylindodicarbocyanine perchlorate, D-307) was purchased from Invitrogen. D-Luciferin was purchased from Gold Biotechnology (St. Louis, MO). Taxol® (Mayne Pharma, Paramus, NJ) and Abraxane® (Abraxis Bioscience, LA, CA) were obtained from a hospital pharmacy.

2.2. Synthesis of PEG^{5k}-CA_8 telodendrimer

PEG^{5k}-CA_8 was synthesized via solution phase condensation reactions from MeO-PEG-NH_2 with a molecular weight of 5000 dalton. (Fmoc)lysine(Fmoc)-OH (2 equ.) was coupled onto the N terminal of PEG using DIC (2 equ.) and HOBt (2 equ.) as coupling reagents in DMF for over night. The completion of the coupling was monitored by Kaiser test: yellow color indicates no amino group left, blue color indicates the presence of amino groups. PEGylated molecules was precipitated by adding cold ether and washed with ether twice. Fmoc groups were removed by the treatment with 20% piperidine in DMF, and the PEGylated molecules were precipitated and washed three times by cold ether. White powder precipitate was dried under vacuum and another two repeat coupling of (Fmoc)lysine(Fmoc)-OH were carried out to generate a third generation of dendritic polylysine on one terminus of PEG. Cholic acid NHS ester, prepared according to the literature[27], was coupled to the terminal end of dendritic

polylysine, resulting in PEG^{5k}-CA_8. This telodendrimer was subsequently dialyzed and lyophilized to yield a white powder.

2.3. Preparation and characterization of PTX/DiD loaded PEG^{5k}-CA_8 nanoparticles

The dry-down or evaporation method was used for PTX loading [9]. PTX and polymer were dissolved in chloroform, and evaporated in rotavapor to obtain a dry polymer-drug film. The film was reconstituted in PBS buffer, followed by sonication for 2 hours, allowing the polymer to self-assemble into PTX-loaded micellar nanoparticles. In this study, the concentration of PEG^{5k}-CA_8 was fixed at 20 mg/mL. Finally, the nanoparticle solution was filtered with a 0.22 μm filter to sterilize the sample. To monitor the real-time biodistribution of PEG^{5k}-CA_8 nanoparticles with optical imaging systems, DiD (hydrophobic NIRF dye) and PTX were co-loaded into the nanocarrier using the same method described as above. The concentration of PTX loaded in PEG^{5k}-CA_8 nanoparticles was measured by HPLC. The mean diameter and zeta potential of the nanoparticles after PTX and DiD loading were evaluated by dynamic light scanning (DLS). The morphology and size distribution of nanoparticles after drug loading were observed using Cryo-Transmission electron microscopy (Cryo-TEM). To determine the *in vitro* drug release profile, PTX loaded PEG^{5k}-CA_8 nanoparticles (2.4 mg/ml) were placed into a dialysis cartridge (molecular weight cutoff = 3 KDa, Thermo Scientific, Rockford, IL). The cartridge was immersed in 1 L PBS and gently shaken at 37 °C at 100 rpm. At different time points, the PBS solution was refreshed and the PTX concentration remained in the dialysis cartridge was measured by HPLC.

2.4. Cell culture

Human foreskin fibroblast (HFF1) cells, and human ovarian clear cell carcinoma cells (ES-2), were purchased from American Type Culture Collection (ATCC; Manassas, VA, USA). Firefly luciferase-expressing ovarian adenocarcinoma cell line (SKOV3-luc-D3) was obtained from Caliper Life Sciences (Hopkinton, MA, USA). All cell lines were cultured in recommended conditions.

2.5. In vitro cytotoxicity

The cytotoxicity of blank PEG^{5k}-CA_8 nanoparticles was evaluated on normal human foreskin fibroblast (HFF1) cells in comparison with the commercial vehicle (Cremophor: Ethanol) in Taxol® formulation. The concentration of blank PEG^{5k}-CA_8 nanoparticles was 20 mg/ml. Commercial dissolvent was prepared with a mixture of Cremphor EL and anhydrous ethanol (50:50 v/v). The methlythiazolyltetrazolium (MTT) assay was used to evaluate cell viability [28]. Briefly, 3×10^3 HFF1 cells in 150 μL culture media were seeded in 96-well plates (Costar, Cambridge, MA) and then incubated for 24 h at 37 °C. Serial dilutions of blank PEG^{5k}-CA_8 nanoparticles or commercial vehicles in a volume of 50 μL were added, and the cells were incubated for 72 h.

The *in vitro* anti-tumor effects of PTX-PEG^{5k}-CA_8 NPs on ES-2 and SKOV3-luc ovarian cancer cell lines were next investigated. The cells were incubated with either PTX-PEG^{5k}-CA_8 NPs, Taxol® or Abraxane® at equivalent PTX concentrations ranging from 0.01 to 10, 000 ng/ml for 72 h. Control cells were incubated with PEG^{5k}-CA_8 NPs without PTX loading at the equivalent NPs concentration. Cell viability was also assessed with MTT assay.

2.6. Animals

Female athymic nude mice (Nu/Nu strain), 6–8 weeks age, were purchased from Harlan (Livermore, CA); female SPF BALB/c mice, 10–12 weeks age, were purchase from Charles River (Davis, CA). All animals were kept under pathogen-free conditions according to AAALAC guidelines and were allowed to acclimatize for at least 4 days prior to any

experiments. All animal experiments were performed in compliance with institutional guidelines and according to protocol No. 06-12262 approved by the Animal Use and Care Administrative Advisory Committee at the University of California, Davis.

2.7. Maximum tolerated dose (MTD) studies

Single dose MTD for PTX-PEG^{5k}-CA$_8$ NPs administered intravenously was investigated in healthy female SPF BALB/c mice. Four groups of five BALB/c mice received single i.v. injections of 75, 100 and 120 mg PTX/kg of the PTX nanoformulation (6.2 mg PTX/mL in 20 mg/mL of PEG^{5k}-CA$_8$), respectively, and PBS as a control. Mice survival and variation in body weight were observed daily for two weeks. At one week after injection, the blood was collected from each mouse to measure blood cell counts and serum chemistry including ALT, AST, total bilirubin, BUN and creatinine. The MTD was defined as the allowance of a median body weight loss of 15% of the control and causes neither death due to toxic effects nor remarkable changes in the general signs within 1 week after administration.

Repeated dose MTD for PTX-PEG^{5k}-CA$_8$ NPs was performed in female nude mice. Four groups of nude mice (n=5) were each injected i.v. with 15, 30, 45 or 60 mg PTX/kg of the PTX nanoformulation (6.2 mg PTX/mL in 20 mg/mL of PEG^{5k}-CA$_8$) once daily for 5 consecutive days. Mice were monitored daily for two weeks.

2.8. Ovarian cancer models development

A subcutaneous xenograft model of ovarian cancer was established by injecting 7×10^6 SKOV3-luc cells in a 100 μL of mixture of PBS and Matrigel (1:1 v/v) subcutaneously (s.c.) at the right flank in female athymic nude mice.

An orthotopic intraperitoneal model of metastatic ovarian cancer was developed by injecting 1×10^7 SKOV3-luc cells (in 400 μL PBS) intraperitoneally (i.p.) into nude mice.

2.9. Biodistribution of PEG^{5k}-CA$_8$ nanoparticles

The *in vivo* biodistribution and tumor targeting ability of PEG^{5k}-CA$_8$ nanoparticles were evaluated by non-invasive optical imaging systems. To monitor the distribution of nanoparitcles in live animals, DiD (NIRF dye) and PTX were co-loaded into PEG^{5k}-CA$_8$ nanoparticles (DiD-PTX-NPs) as described above. Mice with subcutaneous SKOV3-luc tumors of an approximate 8~10 mm diameter were subjected to *in vivo* imaging. 50 nM DiD (dissolved in 1% DMSO) or DiD-PTX-NPs in 100 μL PBS were injected intravenously via the tail vein in tumor bearing mice. At different time points (0.5, 2, 4, 12, 24, 48 and 72 h), mice were anesthetized by intraperitoneal injection of pentobarbitol (60 mg/kg), and scanned using a Kodak multimodal imaging system IS2000MM with an excitation bandpass filter at 625 nm and an emission at 700 nm. Exposure time was 30 s per image. After *in vivo* imaging, animals were euthanized by CO_2 overdose 72 h after injection. Tumors, organs, and muscle tissue were excised and imaged with Kodak imaging station. Fluorescence was determined using operator-defined regions-of-interest (ROI) measurements on tumors and other tissues. Time-dependent tumor contrast profile was determined by the ratio between fluorescence intensities (SI) of tumors and those of normal skin subtracted by the system noise (ROI outside the animal). Data were expressed as mean ± SD (n=3).

$$\text{Tumor/background} = (\text{SI}_{\text{tumor}} - \text{SI}_{\text{noise}})/(\text{SI}_{\text{skin}} - \text{SI}_{\text{noise}})$$

For histological evaluation, excised tumor or muscle specimens were frozen in O.C.T. (embedding medium for frozen tissue) at −80°C, and sectioned into 10 μm slices. The cryosection slides were air-dried and fixed with cold acetone. The nuclei were stained by 4',

6-diamidino-2-phenylindole (DAPI, Invitrogen). The slides were mounted with coverslips and visualized with an Olympus FV1000 laser scanning confocal microscope.

To investigate the PTX-PEG^{5k}-CA$_8$ NPs biodistribution after intraperitoneal injection, DiD-PTX-NPs or free DiD dye were injected i.p. into the mice bearing peritoneally metastatic ovarian cancer xenograft, and their biodistribution were continuously monitored up to 72 h by Kodak imaging system IS2000MM. Finally, the mice were sacrificed and the peritoneal cavity was imaged.

2.10. Therapeutic study

In the subcutaneous ovarian cancer model, treatments were started when tumor in the nude mice reached a tumor volume of 100–200 mm^3 and this day was designated as day 0. On day 0, these mice were randomly divided into five groups (n=5). Mice were administered intravenously with Taxol®, Abraxane®, and PTX-PEG^{5k}-CA$_8$ NPs on days 0, 4, 8 and again on days 38, 42 and 46. Taxol® and Abraxane® were given at their MTDs (13.4 and 30 mg PTX/kg, respectively) [29], and PTX-PEG^{5k}-CA$_8$ NPs were administered at the equivalent PTX doses (13.4 or 30 mg/kg) for comparison. The mice in control group were given PBS only. Tumor sizes were measured with a digital caliper twice per week. Tumor volume was calculated by the formula ($L \times W^2$) /2, where L is the longest, and W is the shortest in tumor diameters (mm). To compare between groups, relative tumor volume (RTV) was calculated at each measurement timepoint (where RTV equals the tumor volume at given timepoint divided by the tumor volume prior to initial treatment). For humane reasons, animals were sacrificed when the implanted tumor volume reached 2,000 mm^3. Mice were imaged noninvasively for luciferase expression every two weeks. Briefly, 150 mg/kg D-luciferin was injected i.p., and mice were anesthetized with pentobarbitol (i.p., 60 mg/kg), bioluminescence imaging was obtained at 15 min post luciferin injection using Kodak imaging station 2000 MM. To monitor potential toxicity, the body weight of each mouse was measured twice weekly. On the third day after the last dosage, blood samples were obtained from all mice for measurement of blood cell counts, ALT, AST, total bilirubin, BUN and creatinine. One mouse from each group was also sacrificed, and its liver submitted for histopathology evaluation.

In the orthotopic intraperintoneal tumor model, drug treatment was initiated three weeks after intraperitoneal implantation of SKOV3-luc cells, when most mice had luminescent signals indicative of peritoneal tumors, and the first treatment day was designated as day 0. The mice were divided into 5 groups (n=5–6), and the mean luminescent intensity was approximately equivalent for all groups. These groups were randomly assigned to receive intraperitoneal injections of PBS control, Taxol® (20 mg/kg), Abraxane® (45 mg PTX/kg), or PTX-PEG^{5k}-CA$_8$ NPs (20 or 45 mg PTX/kg) at day 0, 4, 8, 12, and 16. The tumor response was monitored weekly by noninvasive bioluminescence imaging for luciferase expression. The semiquatitative total bioluminescence (arbitrary unit) was measured by drawing regions of interest (ROIs) around tumor areas enclosing emitted signals. Background was subtracted by measuring same sized ROIs in areas without light emission. Moribund animals were euthanized per protocols. Survival time of the animals was also recorded.

2.11. Statistical analysis

Statistical analysis was performed by Student's t-test for two groups, and one-way ANOVA for multiple groups. All results were expressed as the mean ± standard error (SEM) unless otherwise noted. A value of $P<0.05$ was considered statistically significant.

3. Results

3.1. Preparation and characteration of PTX-PEG^{5k}-CA$_8$ NPs

PEG^{5k}-CA$_8$ telodendrimer, containing eight cholic acids molecules linked to one terminal of a linear PEG molecule (5 KDa) (Fig. 1), was prepared via solution phase condensation reactions. In ^{1}H NMR spectra of PEG^{5k}-CA$_8$, the signal ratio of the protons on PEG to the protons on three methyl groups of cholic acid is 5.925:1, it indicated that eight cholic acid were attached onto a PEG with a molecular weight of 5000 dalton. The molecular weight of PEG^{5k}-CA$_8$ was measured via MALDI-TOF Mass Spectrometry to be 8814 dalton, also indicating eight cholic acid were conjugated onto PEG 5000 (Fig. S-1). The PEG^{5k}-CA$_8$ telodendrimer can self-assemble to form core/shell micellar nanoparticles with 15 nm size in aqueous media. By dry-down method (evaporation method), PTX can be incorporated into polymeric micelles formed by physical entrapment utilizing hydrophobic interactions between PTX and dendritic cholic acid cluster. Loading efficiency (LE) of PTX into PEG^{5k}-CA$_8$ nanoparticles was almost 100% when the initial amount of PTX was < 25 wt.% of PEG^{5k}-CA$_8$ telodendrimer (20 mg/mL), whereas it decreased to 82% and 73% respectively, when the initial amount increased to 33 wt.% and 50 wt.%. The particle size ranged from 20–30 nm when the initial amount was < 25 wt.%, and increased gradually with increasing amount of loaded PTX (Fig. 2). The zeta potential of PTX-PEG^{5k}-CA$_8$ NPs was almost neutral (−1.62 mv to 1.46 mv). To visualize the biodistribution of PEG^{5k}-CA$_8$ *in vivo*, DiD (D-307, a near infra-red (NIR) fluorescent dye) along with PTX were encapsulated into the nanoparticles at the concentrations of 0.5 mg/ml and 4.2 mg/ml, respectively. The particle size of PEG^{5k}-CA$_8$ nanoparticles loaded with DiD and PTX was 56 nm as measured by the dynamic light scanning (DLS) method (Fig. 3A). Cryo-TEM images showed the particles were spherical *in situ*, and the sizes were 50–60 nm (Fig. 3B), which was consistent with the results obtained by DLS.

Using a membrane dialysis method, PTX-PEG^{5k}-CA$_8$ NPs was found to exhibit sustained drug release into surrounding PBS, with rapid release of 20% of the drug in the first 2 h, and cumulative release of 35% of the drug by 12 h, after which there was a slow linear release of 75% of the drug by 156 h (Fig. S-2). PTX-PEG^{5k}-CA$_8$ NPs have also been found to be very stable at 4 °C, showing no significant changes in average particle size over 6 months. Whereas, Abraxane® was unstable and start to form larger aggregates and precipitate 4 days after dissolving the white powder of Abraxane with saline (Fig. S-3).

3.2. In vitro cytotoxicity of PEG^{5k}-CA$_8$ NPs

Blank PEG^{5k}-CA$_8$ NPs were evaluated for their cytotoxicity against normal human fibroblast (HFF1) cells with an MTT assay. As shown in Fig. 4A, compared to the severe toxicity from the commercial vehicle (Cremophor:ethanol 1:1 v/v) at the estimated concentration (9 mg/mL) after blood dilution in clinicical settings [30], our drug carrier did not exhibit detectable cytotoxicity at all the concentrations up to 2 mg/ml (the estimated blood concentratrion after *in vivo* adiministration is about 0.2 mg/ml).

The *in vitro* anticancer activity of the PTX-PEG^{5k}-CA$_8$ NPs (continuous exposure of drug) was performed on ES-2 and SKOV3-luc ovarian cancer cells and compared with Taxol®and Abraxane®. As shown in Fig. 4 B and C, similar dose-response curves were observed in both ES-2 and SKOV3-luc cells for all three PTX formulations. Furthermore, the IC$_{50}$ values of PTX-PEG^{5k}-CA$_8$ NPs were comparable to those of Taxol®and Abraxane® in these two ovarian cancer cells at 72 h, indicating PTX-PEG^{5k}-CA$_8$ NPs exhibited equivalent cytotoxic activity *in vitro*. Additionally, there was no cellular toxicity caused by the blank PEG^{5k}-CA$_8$ NPs (without PTX) at the studied NPs concentration range, eliminating the possibility that nanoparticles themselves were responsible for the cytotoxicity.

3.3. Maximum Tolerated Dose

MTD studies for PTX-PEG^{5k}-CA$_8$ NPs were carried out in non-tumor bearing mice. In the single dose study, the body weight loss in 75 mg PTX/kg PTX-PEG^{5k}-CA$_8$ NPs group was less than 10%, and the white and red blood cell counts and serum chemistry (hepatic and renal function tests panel) were all within normal range, and no histopathologic change was observed in major organs such as lung, liver and spleen, while 2 of 5 mice received 100 mg PTX/kg PTX-PEG^{5k}-CA$_8$ and all the mice received 120 mg PTX/kg PTX-PEG^{5k}-CA$_8$ died. Thus the single dose MTD for PTX-PEG^{5k}-CA$_8$ NPs was between 75 and 100 mg PTX/kg in BALB/c mice. In the repeated dose toxicity study, nude mice were injected with different PTX-PEG^{5k}-CA$_8$ NPs doses via tail vein once daily for 5 consecutive days. The repeated dose MTD for PTX-PEG^{5k}-CA$_8$ NPs in nude mice was approximately 45 mg PTX/kg.

3.4. In vivo biodistribution of PEG^{5k}-CA$_8$ NPs in tumor bearing mice

Non-invasive NIR fluorescence optical imaging technology was utilized to monitor the real-time distribution, excretion, and tumor targeting efficiency of DiD fluorescence labeled PEG^{5k}-CA$_8$ NPs in mice bearing s.c. SKOV3-luc ovarian cancer xenograft. NIRF dyes enable deep tissue imaging with high penetration, low tissue absorption and scattering [31]. Equivalent amount of free DiD dye or DiD-PTX-NPs were injected via the tail vein into s.c. SKOV3-luc tumor bearing mice. The entire animal became fluorescent immediately after nanoparticle administration, and substantial contrast between subcutaneous tumor and normal tissue was observed from 4 to 72 h post-injection (Fig. 5A). Based on imaging results, a semiquantitative time-dependent tumor/background contrast profile was derived from the average fluorescence intensities of equal areas within tumor and normal skin tissue regions (Fig. 5C). PEG^{5k}-CA$_8$ nanoparticles uptake in tumors increased gradually compared to normal tissue following injection, reached the peak at 12 h, and maintained a strong fluorescence signal up to 72 h. This demonstrated that PEG^{5k}-CA$_8$ nanoparticles could preferentially accumulated in tumors compared to normal tissue, likely due to the prolonged circulation and enhanced permeability and retention (EPR) effects. In comparison, no obvious tumor/background contrast in fluorescence intensity was observed all the time in mice injected with free DiD dye, thereby excluding the possibility of tumor targeting effect mediated by DiD dye alone. At 72 h post injection, tumors and major organs were excised for *ex vivo* NIRF imaging to determine PEG^{5k}-CA$_8$ nanoparticle tissue distribution. As shown in Fig. 5B, PEG^{5k}-CA$_8$ nanoparticles mainly accumulated in the tumor tissue, which exhibited strong NIR fluorescence intensity, almost 5-fold higher than the tumor uptake of free DiD control ($P<0.05$, Fig. 5D). However PEG^{5k}-CA$_8$ nanoparticle uptake was not predominant in normal tissue except liver, indicating the decisive evidence of tumor targeting ability of PEG^{5k}-CA$_8$ nanoparticles. This was further confirmed in the microscopic analysis, which showed that the fluorescence signal of PEG^{5k}-CA$_8$ nanoparticles in the tumor was much stronger than that in muscle normal tissue (Fig. 5E). It is not surprising that there is a relatively high uptake in the liver compared to other organs, since most macromolecules larger than the renal cut-off size (10 nm) [8] are eliminated predominately via reticuloendothelial system uptake such as Kupffer cells in the liver.

PEG^{5k}-CA$_8$ nanoparticles biodistribution after i.p. injection in intraperitoneal SKOV3-luc ovarian tumor bearing mice was investigated. Mice were injected i.p. with free DiD or DiD-labeled PEG^{5k}-CA$_8$ nanoparitcles. In mice treated with free DiD, fluorescence rapidly diffused throughout the body post injection and declined to a level not distinguishable from background auto-fluorescence at 72 h (data not shown). In contrast, mice injected with DiD-labeled PEG^{5k}-CA$_8$ nanoparticles resulted in strong fluorescence mainly localized in the abdominal region, with a majority still present at 72 h (Fig. 6A). At 72 h, the peritoneal cavity was exposed and scanned with the Kodak imaging station, displaying DiD-labeled PEG^{5k}-CA$_8$ nanoparticles localization on the surface of peritoneal tumor nodules (Fig. 6B).

3.5. Anti-tumor efficacy and toxicity study after intravenous therapy in a subcutaneous ovarian tumor xenograft model

The anti-tumor effects of PTX-PEG^{5k}-CA$_8$ NPs after intravenous injection were evaluated in subcutaneous SKOV3-luc tumor bearing mice. PBS, Taxol® (13.4 mg/kg), Abraxane® (30 mg PTX/kg) and PTX-PEG^{5k}-CA$_8$ NPs (13.4 and 30 mg PTX/kg), were administered on days 0, 4, 8 (first course). Tumor growth was inhibited in mice treated with all the PTX formulations with the PTX-PEG^{5k}-CA$_8$ NPs at 30 mg PTX/kg being the most effective ; however, tumor progression was subsequently noted in all these treatment groups. There, a second treatment cycle was initiated on day 38. Overall, mice showed decreased tumor growth rate after the intravenous administration of Taxol®, Abraxane® and PTX-PEG^{5k}-CA$_8$ NPs (Fig. 7A). However, PTX-PEG^{5k}-CA$_8$ exhibited superior anti-tumor activity as compared with Taxol®. By day 73, the median RTV was 14.9 for Taxol, while the RTVs for 13.4 mg PTX/kg PTX-PEG^{5k}-CA$_8$ NPs, Abraxane and 30 mg PTX/kg PTX-PEG^{5k}-CA$_8$ NPs were 10.7, 7.9 and 5, respectively ($P<0.05$ for all). Furthermore, there was a single complete response noted in the 30 mg PTX/kg PTX-PEG^{5k}-CA$_8$ NPs group, but no complete responses in any other groups.

Bioluminescence imaging was also utilized to detect luciferase-expressing cancer cells and to monitor the viability and metastasis of tumor cells. As shown in Fig. S-4 C, the pseudocolor images visually demonstrated the differential growth of subcutaneous tumors in different treatment groups. The total emitted bioluminescence intensity (arbitrary units) was measured (Fig. S-4 A), and displayed a good correlation ($R^2=0.84$) between tumor size and bioluminescence data (Fig. S-4 B).

Toxicities were assessed by analyzing effects on animal behavior, body weight change, blood cell counts, and hepatic and renal functions. It was noted that mice receiving Taxol® treatment frequently demonstrated decreased overall activity over 10 min post injection, whereas no noticeable change in activity was observed after administration of either dose of PTX-PEG^{5k}-CA$_8$ NPs. This behavioral difference observed in the Taxol® group may be related to the use of Cremophor EL and ethanol as vehicle of paclitaxel [32]. The Taxol® group exhibited significant body weigh loss during both treatment cycles ($P<0.05$), while the body weight didn't decrease in the PTX-PEG^{5k}-CA$_8$ NPs groups (Fig. 7B). On day 3 post the last injection, blood samples were collected for blood cell counts and serum chemistry measurement. WBC, RBC, and platelet counts in all the groups were within the normal range and excluded the potential hematologic toxicity (Table S-1). The serum chemistry (ALT, AST, Total bilirubin, BUN and Creatinine) in all the groups were also within the normal range, indicating an absence of hepatic and renal toxicity (Table S-2). Histological examination of the liver further confirmed the absence of hepatotoxicity (Fig. S-5).

3.6. Intraperitoneal therapy in an orthotopic ovarian cancer model

Given that a majority of ovarian cancer is diagnosed and treated at advanced stages, diffuse carcinomatosis throughout the intraperitoneal cavity is frequently observed. For those women with optimally debulked cancer, intraperitoneal chemotherapy has demonstrated a therapeutic advantage over intravenous therapy alone [33]. This therapeutic benefit is thought to be conferred by the relatively high local concentrations in the peritoneal cavity after i.p. administration. As shown in the biodistribution study above, PTX-PEG^{5k}-CA$_8$ NPs after i.p. injection could remain in the peritoneal cavity, thereby exposing metastatic intraperitoneal tumor nodules and deposits to higher concentrations of the chemotherapeutic drug. Therefore, the therapeutic efficacy of PTX-PEG^{5k}-CA$_8$ NPs after i.p. therapy was evaluated and compared with Taxol® and Abraxane® in the orthotopic murine model of peritoneally metastatic ovarian cancer. Nude mice bearing i.p. metastatic SKOV3-luc ovarian tumor xenograft were injected i.p. with Taxol® (20 mg/kg), Abraxane® (45 mg PTX/kg) and PTX-PEG^{5k}-CA$_8$ (20 and 45 mg PTX/kg) for total 5 doses on day 0, 4, 8, 12 and 16. Bioluminescence imaging was

performed weekly after treatment, and tumor bioluminesce was quantified by measuring pseudocolor intensity (Fig. 8A). Compared with the control group, mice in all the treatment groups displayed significantly slower increase rates of light intensity ($P<0.05$). Among treatment groups, light intensities in PTX-PEG^{5k}-CA_8 groups were lower than those of Taxol® and Abraxane® at equivalent PTX doses. Notably, one mouse in 20 mg PTX/kg PTX-PEG^{5k}-CA_8 NPs group and two mice in 45 mg PTX/kg PTX-PEG^{5k}-CA_8 NPs group experienced complete responses to therapy prior to subsequent relapses. Conversely, none of the mice treated with Taxol® demonstrated complete responses (Fig. 8C). All mice were also followed to determine the length of survival. Median survival time was 39 days (range 29–45) for untreated mice in the PBS control group, while the median survival time was significantly extended with all three PTX formulations treatment ($P<0.001$). However, PTX-PEG^{5k}-CA_8 NPs treatment exhibited greater survival benefit than Taxol® and Abraxane® at equivalent PTX doses. Median survival time for the Taxol® group was 65 days (range 37–81) and 74 days (range 49–92) for the 20 mg PTX/kg PTX-PEG^{5k}-CA_8 NPs group. Median survival was 81 days (range 55–90) for the Abraxane® group and 85 days (range 66–105+) for the 45 mg PTX/kg PTX-PEG^{5k}-CA_8 NPs group (Fig. 8B).

4. Discussion

Polymeric micelles are one of the most promising nanocarriers due to their unique core-shell structure, which could “solubilize” hydrophobic drug molecules under aqueous condition by physical encapsulation [34]. In addition to improve the poor solubility associated with many cancer chemotherapeutic drugs such as PTX, nanocarriers can also prolong the circulation time, achieve controlled and sustained drug release, and accumulate in the tumor sites, thereby maximizing the therapeutic index and minimizing nonspecific toxicity. There are several key factors which can affect their fates *in vivo*, the magnitude and pattern of tumoral distribution of nanoparticles, including their *in vivo* colloidal stability, particle size, and surface characteristics [35]. Many nanoparticles have been investigated for their potential use in drug delivery; however, only a few such as Doxil® (Doxorubicin liposomal) and Abraxane® (Albumin-bound paclitaxel) have been approved by FDA. The particle sizes for Doxil® and Abraxane® are 150 and 130 nm, respectively. Their relatively large sizes may hinder diffusion in the extracelluar space in the tumors, and thereby serve to limit their effectiveness in the treatment of solid tumors [36]. It has been reported that the optimal nanoparticle size for tumor penetration should be less than 100 nm [8].

In this study, a well-defined copolymer (telodendrimer) composed of PEG, lysine and cholic acid (PEG^{5k}-CA_8) was successfully developed, which can encapsulate PTX and self-assemble to form micelles in water solution, and has been tested for targeted drug delivery in the treatment of ovarian cancer. The PEG^{5k}-CA_8 telodendrimer has shown to possess many promising features such as high drug loading capacity, relatively small particle size (20–60 nm) after drug loading, sustained drug release profile, and superior stabliliy. The azide group at the distal terminus of PEG chain provides a reactive site for the conjugation of tumor cell surface or tumor endothelial cell surface binding ligands so that tumor targeting nanoparticles can be developed. These dendrimers also can be synthesized and prepared in large amount as monodispersed populations, preventing potential batch-to-batch variance.

The three building blocks for the telodendrimer including PEG, lysine, and cholic acid are all nontoxic. Our *in vitro* cytotoxicity study demonstrated that no cytotoxicity of blank PEG^{5k}-CA_8 NPs (up to 2 mg/ml) was observed in normal human fibroblast HFF1 cells. In contrast, the commercial vehicle for PTX, the mixture of Cremophor and ethanol (1:1), had severe cytotoxicity to HFF cells at the clinically relevant blood concentration. When PEG^{5k}-CA_8 NPs were loaded with PTX, they showed similar cytotoxicity to ES-2 and SKOV-3 ovarian cancer cells compared with Taxol®, suggesting that PTX can be released from the nanoparticles and

achieve tumor cell killing efficacy. PTX-PEG^{5k}-CA$_8$ NPs have demonstrated better safety profiles *in vivo* than Taxol® or even Abraxane®. The MTD of PTX-PEG^{5k}-CA$_8$ NPs after single dose in BALB/c mice was between 75 and 100 mg PTX/kg, 2.5 times higher than that of Taxol (30 mg/kg) [37]. The MTD of PTX-PEG^{5k}-CA$_8$ NPs after five consecutive doses in nude mice was approximately 45 mg PTX/kg, whereas that of Taxol® and Abraxane® were reported to be 13.4 and 30 mg PTX/kg, respectively [29].

Noninvasive NIRF optical imaging technology was used to real-time monitor the biodistrubiton and tumor accumulation of PTX-PEG^{5k}-CA$_8$ NPs after administration. Hydrophobic NIFR dye DiD was encapsulated along with PTX in PEG^{5k}-CA$_8$ NPs to visualize the fates of nanoparticles in live animals. PTX-PEG^{5k}-CA$_8$ nanoparticles post i.v. injection in SKOV3-luc ovarian cancer bearing mice have shown to have a prolonged blood circulation time, and preferentially accumulate in tumors, possibly as a result of EPR effects. Notablly, the nanoparticles distributed throughout the tumors, as observed in the confocal microscopy analysis of tumor cryosection, which meant the nanoparticles had a good tumor penetration, likely attributed in part to their relatively small sizes (around 50 nm). It has been reported that although some naoparticles with larger size such as liposomes can be delivered effectively to a solid tumor via the EPR effect, they would not be distributed sufficiently to cancer cells distant from tumor vessels [38]. The biodistribution of PEG^{5k}-CA$_8$ NPs after i.p. injection was also investigated in orthotopic intraperitoneal metastatic SKOV3-luc ovarian cancer model. The results demonstrated that the PEG^{5k}-CA$_8$ drug carrier significantly extended the residence time of paclitaxel in the peritoneal cavity, reducing the rate and extent of drug absorption from the cavity into systemic circulation. This may result in sustained and enhanced drug exposure to the ovarian tumors localized in the peritoneal cavity. A possible explanation may be that the rapidly-growing ovarian tumor cells block the lymphatic drainage, and likely restrict PEG^{5k}-CA$_8$ NPs to the peritoneum [39].

The anti-tumor efficacy of PTX-PEG^{5k}-CA$_8$ NPs was evaluated after i.v. therapy in subcutaneous ovarian cancer model and i.p. therapy in the orthotopic i.p. metastatic ovarian cancer model. PTX-PEG^{5k}-CA$_8$ NPs exhibited superior toxicity profiles and higher antitumor activity in both ovarian cancer models as compared with Taxol® or Abraxane® at equivalent PTX doses. There are several possible explanations for enhanced efficacy and relatively lower toxicity of PTX-PEG^{5k}-CA$_8$ NPs after intravenous injection. First, the PEG^{5k}-CA$_8$ nanocarrier may improve the pharmacokinetic profile of PTX, prolonging its circulation time, thus resulting in a higher accumulation in tumors due to EPR effects. Secondly, since PTX-PEG^{5k}-CA$_8$ NPs accumulate in tumor, PTX is released in a sustained manner so that tumor cells can be exposed to PTX for longer time period. Thirdly, PTX-PEG^{5k}-CA$_8$ NPs have a relatively smaller size (50 nm) compared to Abraxane (130 nm), which may result in deeper penetration into tumor nodules, as confirmed by confocal microscopy images. Although some uptake of the nanoparticle by the liver was observed through NIRF imaging, the culprit responsible for the nonspecific uptake is most likely the Kupffer cells in liver. There was no evidence of hepatoxicity in mice received repeated dose of PTX-PEG^{5k}-CA$_8$ NPs, as confirmed in both serum chemistry and histological examination.

Intraperitoneal therapy of PTX has already demonstrated survival advantages in the treatment of human ovarian cancer, but its use is limited by several complications, including infection due to prolonged use of indwelling catheter and local toxicity (e.g., abdominal pain and other gastrointestinal toxicities) [40]. As shown in this study, the PEG^{5k}-CA$_8$ drug carrier affected the biodistribution of PTX after intraperitoneal injection and demonstrated a sustained drug release profile, resulting in enhanced efficacy and better tolerability in then peritoneally metastatic ovarian cancer mice model when compared to Taxol®.

5. Conclusions

In summary, a well-defined nontoxic copolymer (telodendrimer) composed of the PEG and unique amphiphilic molecule (cholic acid) was successfully developed, which can readily encapsulate hydrophobic drugs such as PTX and self-assemble to form stable micellar nanoparticles. PTX loaded nanoparticles had prolonged circulation time and accumulated preferentially in ovarian tumors via EPR effects, which resulted in enhanced therapeutic efficacy with better safety profiles in our subcutaneous and orthotopic ovarian cancer models when compared to Taxol® or Abraxane® alone. Therefore, the PEG-CA telodendrimer based micellar nanoparticle is a promising drug delivery system for hydrophobic drugs such as PTX in the treatment of cancer.

Supplementary Material

Refer to Web version on PubMed Central for supplementary material.

Acknowledgements

The authors thank the editorial assistance provided by David Olivos and Mary Saunders, the financial support from NIH/NCI NCDDG U19 CA113298, R21CA128501, RO1CA115483, and China Scholarship Council (CSC).

References

1. Goff BA, Mandel L, Muntz HG, Melancon CH. Ovarian carcinoma diagnosis. Cancer 2000;89(10): 2068–2075. [PubMed: 11066047]
2. Rowinsky EK, Cazenave LA, Donehower RC. Taxol: a novel investigational antimicrotubule agent. J Natl Cancer Inst 1990;82(15):1247–1259. [PubMed: 1973737]
3. Anon. Paclitaxel (taxol) for ovarian cancer. Med Lett Drugs Ther 1993;35(896):39–40. [PubMed: 8097551]
4. Weiss RB, Donehower RC, Wiernik PH, Ohnuma T, Gralla RJ, Trump DL, et al. Hypersensitivity reactions from taxol. J Clin Oncol 1990;8(7):1263–1268. [PubMed: 1972736]
5. Devalapally H, Duan Z, Seiden MV, Amiji MM. Modulation of drug resistance in ovarian adenocarcinoma by enhancing intracellular ceramide using tamoxifen-loaded biodegradable polymeric nanoparticles. Clin Cancer Res 2008;14(10):3193–3203. [PubMed: 18483388]
6. Kingsley JD, Dou H, Morehead J, Rabinow B, Gendelman HE, Destache CJ. Nanotechnology: a focus on nanoparticles as a drug delivery system. J Neuroimmune Pharmacol 2006;1(3):340–350. [PubMed: 18040810]
7. Matsumura Y, Maeda H. A new concept for macromolecular therapeutics in cancer chemotherapy: mechanism of tumoritropic accumulation of proteins and the antitumor agent smancs. Cancer Res 1986;46(12 Pt 1):6387–6392. [PubMed: 2946403]
8. Davis ME, Chen ZG, Shin DM. Nanoparticle therapeutics: an emerging treatment modality for cancer. Nat Rev Drug Discov 2008;7(9):771–782. [PubMed: 18758474]
9. Liu J, Lee H, Allen C. Formulation of drugs in block copolymer micelles: drug loading and release. Curr Pharm Des 2006;12(36):4685–4701. [PubMed: 17168772]
10. Tong R, Cheng J. Anticancer Polymeric Nanomedicines. Polymer Reviews (Philadelphia, PA, United States) 2007;47(3):345–381.
11. Trubetskoy VS. Polymeric micelles as carriers of diagnostic agents. Advanced Drug Delivery Reviews 1999;37(1–3):81–88. [PubMed: 10837728]
12. Liggins RT, Burt HM. Polyether-polyester diblock copolymers for the preparation of paclitaxel loaded polymeric micelle formulations. Adv. Drug Deliv. Rev 2002;54(2):191–202. [PubMed: 11897145]
13. Le Garrec D, Ranger M, Leroux J-C. Micelles in anticancer drug delivery. Am. J. Drug Deliv 2004;2 (1):15–42.
14. Zhang X, Jackson JK, Burt HM. Development of amphiphilic diblock copolymers as micellar carriers of taxol. Inter. J. Pharm 1996;132(12):195–206.

15. CT M, HG L, ME J, SK A. J Am Chem Soc 1994;116:11195.
16. van Hest JCM, Delnoye DAP, Baars MWPL, van Genderen MHP, Meijer EW. Polystyrene-dendrimer amphiphilic block copolymers with a generation-dependent aggregation. Science 1995;268(5217): 1592–1595. [PubMed: 17754610]
17. Gillies ER, Jonsson TB, Frechet JMJ. Stimuli-Responsive Supramolecular Assemblies of Linear-Dendritic Copolymers. J. Am. Chem. Soc 2004;126(38):11936–11943. [PubMed: 15382929]
18. Chang Y, Kwon YC, Lee SC, Kim C. Amphiphilic Linear PEO-Dendritic Carbosilane Block Copolymers. Macromolecules 2000;33(12):4496–4500.
19. Gitsov I, Wooley KL, Hawker CJ, Ivanova PT, Frechet JMJ. Synthesis and properties of novel linear-dendritic block copolymers. Reactivity of dendritic macromolecules toward linear polymers. Macromolecules 1993;26(21):5621–5627.
20. Iyer J, Fleming K, Hammond PT. Synthesis and Solution Properties of New Linear-Dendritic Diblock Copolymers. Macromolecules 1998;31(25):8757–8765.
21. TV P. Self-assembling complexes for gene delivery: from laboratory to clinical trial. 1998:277.
22. Lee CC, Gillies ER, Fox ME, Guillaudeu SJ, Frechet JM, Dy EE, et al. A single dose of doxorubicin-functionalized bow-tie dendrimer cures mice bearing C-26 colon carcinomas. Proc Natl Acad Sci U S A 2006 Nov 7;103(45):16649–16654. [PubMed: 17075050]
23. Gillies ER, Frechet JM. pH-Responsive copolymer assemblies for controlled release of doxorubicin. Bioconjug Chem 2005 Mar–Apr;16(2):361–368. [PubMed: 15769090]
24. Vijayalakshmi N, Maitra U. A simple construction of a bile acid based dendritic light harvesting system. Org Lett 2005;7(13):2727–2730. [PubMed: 15957932]
25. Gref R, Minamitake Y, Peracchia MT, Trubetskoy V, Torchilin V, Langer R. Biodegradable long-circulating polymeric nanospheres. Science 1994;263(5153):1600–1603. [PubMed: 8128245]
26. Blume G, Cevc G. Liposomes for the sustained drug release in vivo. Biochim Biophys Acta 1990;1029 (1):91–97. [PubMed: 2223816]
27. Pandey PS, Rai R, Singh RB. Synthesis of cholic acid-based molecular receptors: head-to-head cholaphanes. J Chem Soc, Perkin Trans 1 2002;(7):918–923.
28. Mosmann T. Rapid colorimetric assay for cellular growth and survival: application to proliferation and cytotoxicity assays. J Immunol Methods 1983;65(1–2):55–63. [PubMed: 6606682]
29. Desai N, Trieu V, Yao Z, Louie L, Ci S, Yang A, et al. Increased antitumor activity, intratumor paclitaxel concentrations, and endothelial cell transport of cremophor-free, albumin-bound paclitaxel, ABI-007, compared with cremophor-based paclitaxel. Clin Cancer Res 2006;12(4):1317–1324. [PubMed: 16489089]
30. Bilensoy E, Gurkaynak O, Dogan AL, Hincal AA. Safety and efficacy of amphiphilic beta-cyclodextrin nanoparticles for paclitaxel delivery. Int J Pharm 2008;347(1–2):163–170. [PubMed: 17689901]
31. Peng L, Liu R, Marik J, Wang X, Takada Y, Lam KS. Combinatorial chemistry identifies high-affinity peptidomimetics against alpha4beta1 integrin for in vivo tumor imaging. Nat Chem Biol 2006;2(7): 381–389. [PubMed: 16767086]
32. Kim SC, Kim DW, Shim YH, Bang JS, Oh HS, Wan Kim S, et al. In vivo evaluation of polymeric micellar paclitaxel formulation: toxicity and efficacy. J Control Release 2001;72(1–3):191–202. [PubMed: 11389998]
33. de Bree E, Theodoropoulos PA, Rosing H, Michalakis J, Romanos J, Beijnen JH, et al. Treatment of ovarian cancer using intraperitoneal chemotherapy with taxanes: from laboratory bench to bedside. Cancer Treat Rev 2006;32(6):471–482. [PubMed: 16942841]
34. Matsumura Y. Poly (amino acid) micelle nanocarriers in preclinical and clinical studies. Adv Drug Deliv Rev 2008;60(8):899–914. [PubMed: 18406004]
35. Cho YW, Park SA, Han TH, Son DH, Park JS, Oh SJ, et al. In vivo tumor targeting and radionuclide imaging with self-assembled nanoparticles: mechanisms, key factors, and their implications. Biomaterials 2007;28(6):1236–1247. [PubMed: 17126900]
36. Dreher MR, Liu W, Michelich CR, Dewhirst MW, Yuan F, Chilkoti A. Tumor vascular permeability, accumulation, and penetration of macromolecular drug carriers. J Natl Cancer Inst 2006;98(5):335–344. [PubMed: 16507830]

37. Straubinger RM, Sharma A, Murray M, Mayhew E. Novel Taxol formulations: Taxol-containing liposomes. J Natl Cancer Inst Monogr 1993;(15):69–78. [PubMed: 7912532]

38. Unezaki S, Maruyama K, Hosoda J, Nagai I. Direct measurement of the extravasation of polyethylene glycol-coated liposomes into solid tumour tissue by in vivo fluorescence microscopy. Int J Pharmacol 1996;144(1):11–17.

39. Sharma A, Sharma US, Straubinger RM. Paclitaxel-liposomes for intracavitary therapy of intraperitoneal P388 leukemia. Cancer Lett 1996;107(2):265–272. [PubMed: 8947523]

40. Tsai M, Lu Z, Wang J, Yeh TK, Wientjes MG, Au JL. Effects of carrier on disposition and antitumor activity of intraperitoneal Paclitaxel. Pharm Res 2007;24(9):1691–1701. [PubMed: 17447121]

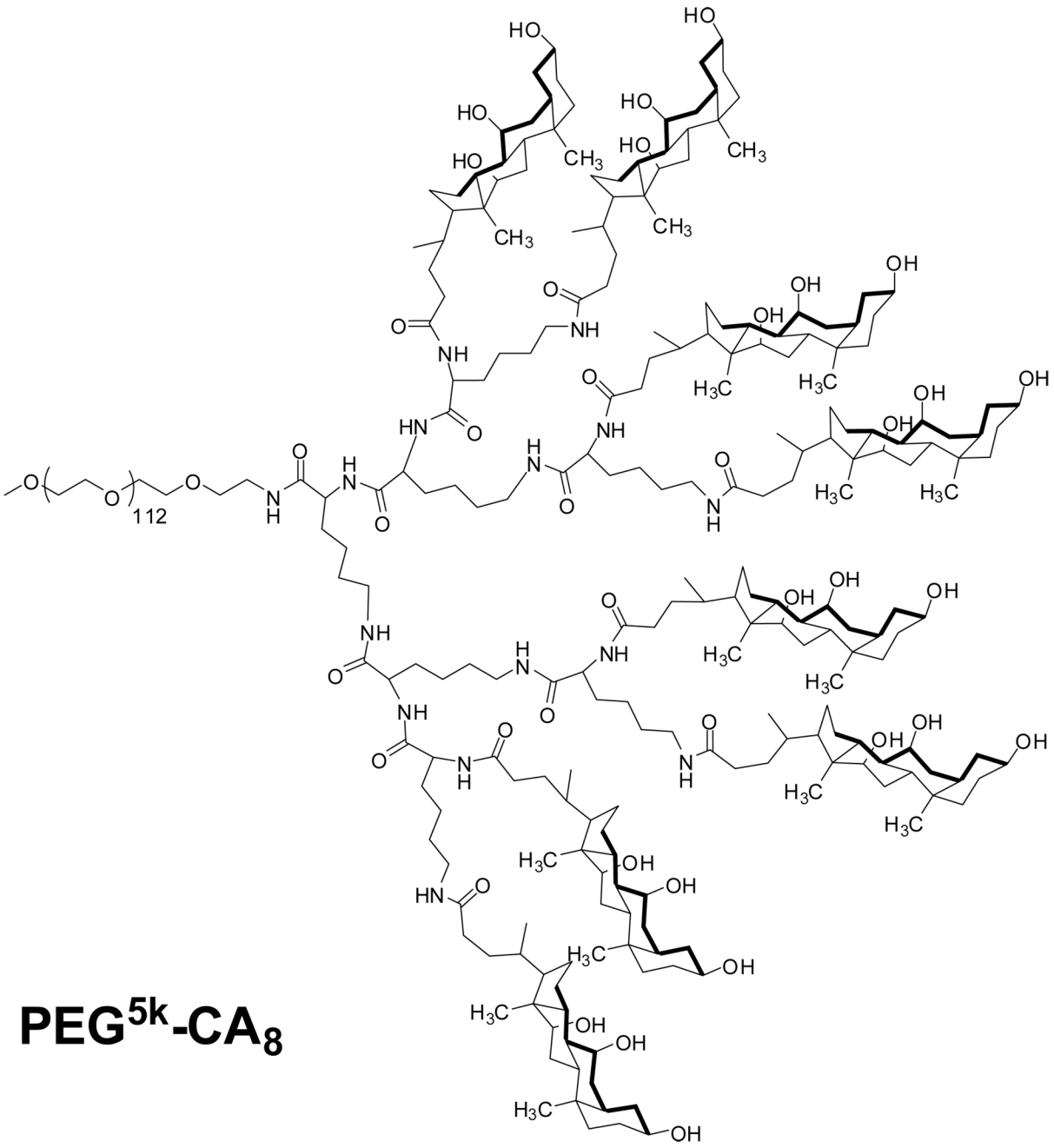

Fig. 1.
The chemical structure of PEG^{5k}-CA_8 telodendrimer.

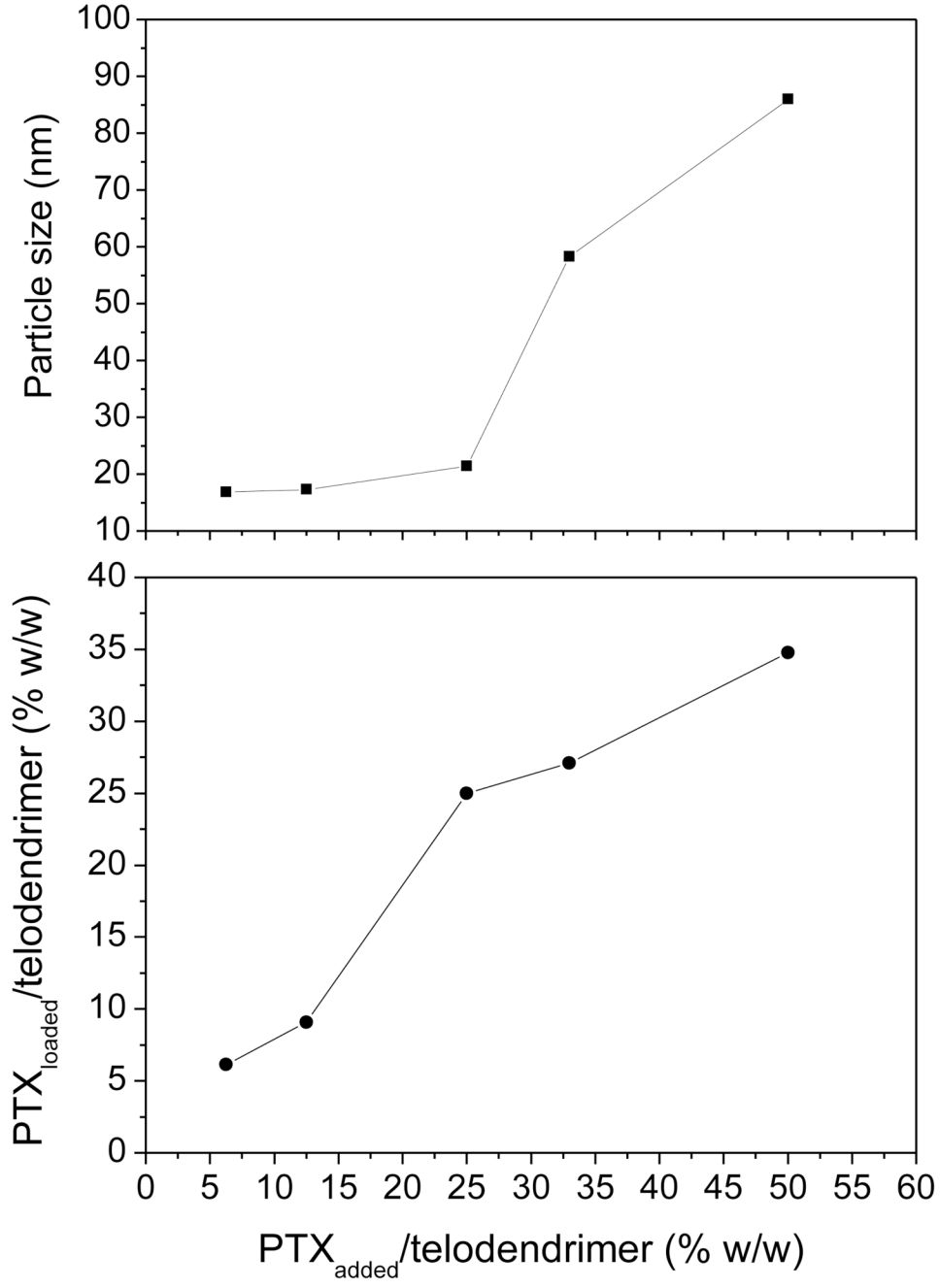

Fig. 2.

The relationships of the particle size of the PTX-PEG^{5k}-CA$_8$ micelles (top) and the PTX/telodendrimer ratios in PTX-PEG^{5k}-CA$_8$ micelles (bottom) *vs* the feed ratios of PTX/telodendrimer during the drug loading, respectivley. The concentration of PEG^{5k}-CA$_8$ telodendrimer was 20 mg/mL.

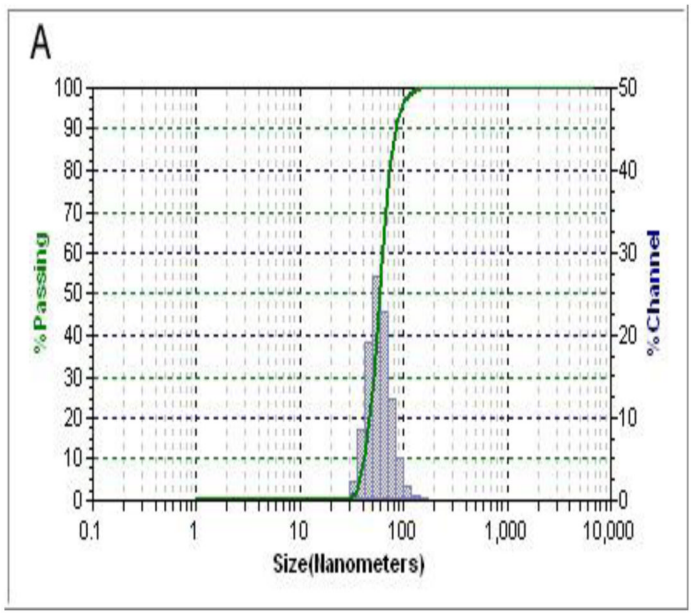

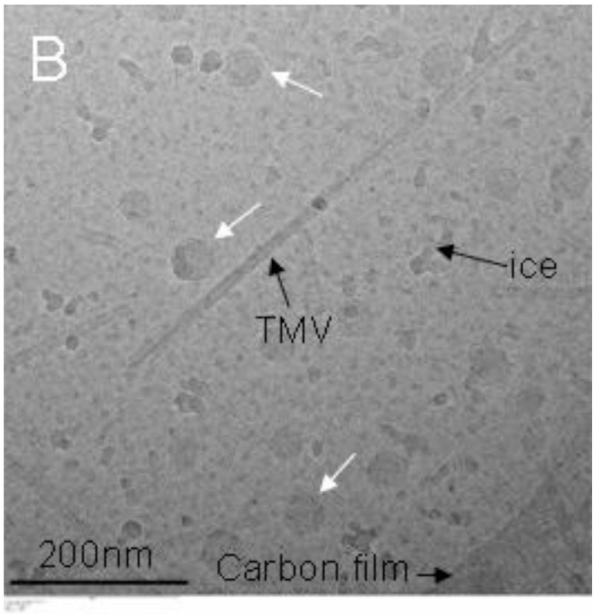

Fig. 3.

The size distribution of PEG^{5k}-CA_8 nanoparticles loaded with PTX and NIRF dye DiD in PBS measured by dynamic light scanning (DLS) (A) and Cryo-Transmission electron microscopy (Cryo-TEM) (B). In Fig. 3B, white arrows point to nanoparticles, while Tubacco Mosaic Virus (TMV) was used as calibration standard (18 nm in width).

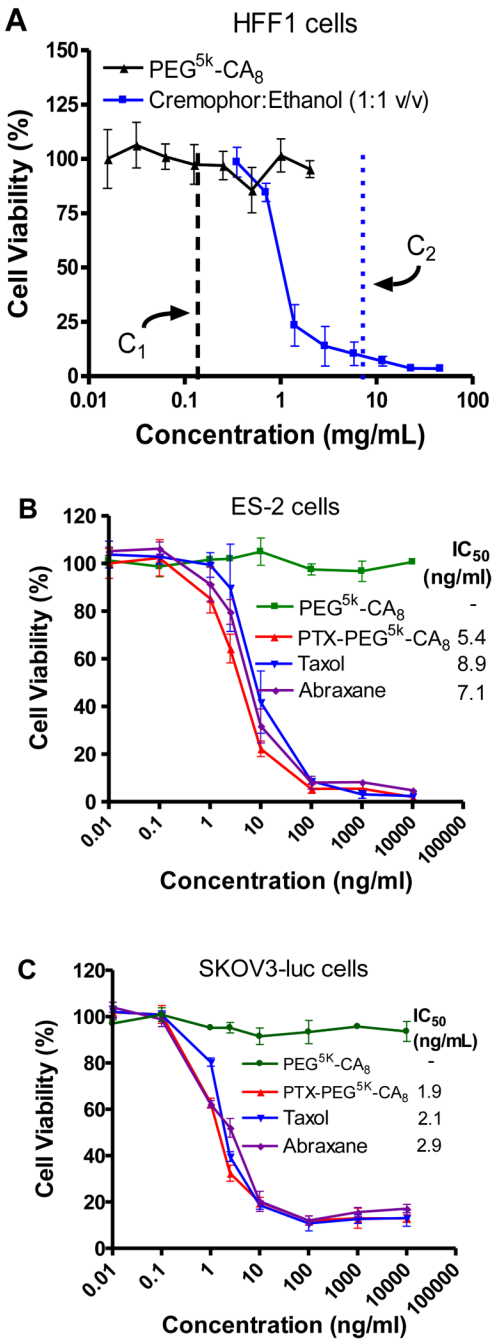

Fig. 4.

The cytotoxicity of PEG^{5k}-CA_8 nanoparticles with or without PTX loading against normal human cells and ovarian cancer cells. (A) Cytotoxicity of blank PEG^{5k}-CA_8 NPs and cremophor:ethanol vehicle on HFF1 human fibroblast cells. C_1 and C_2 are the estimated blood concentratoin of PEG^{5k}-CA_8 and cremophor:ethanol after *in vivo* administration, respectively, assuming the blood volume of an average person is 6L. The anticancer effects of PTX-loaded PEG^{5k}-CA_8 NPs were performed on ES-2 cells (B) and SKOV3-luc cells (C) compared with Taxol®and Abraxane®.

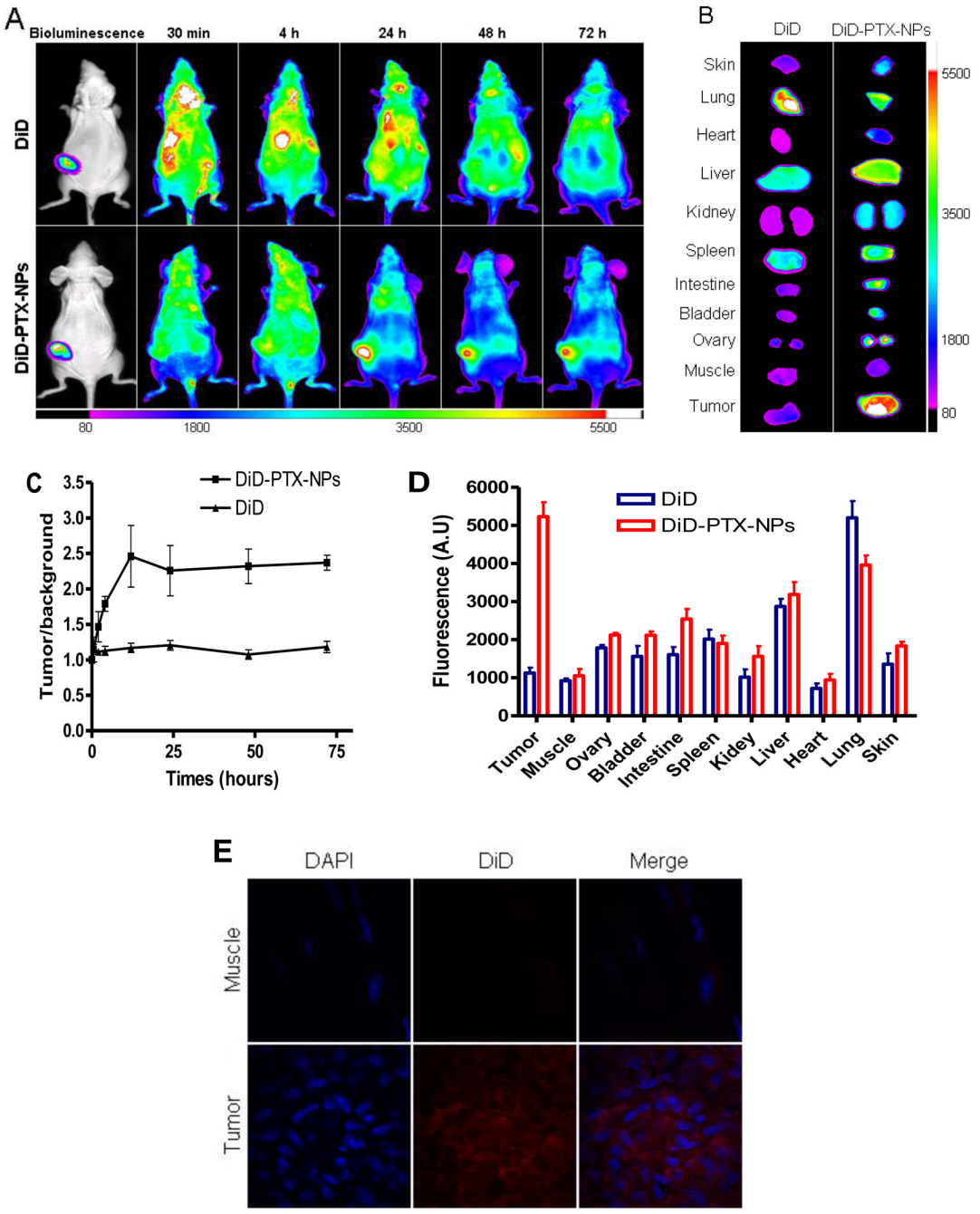

Fig. 5.

In vivo and *ex vivo* NIRF imaging of PEG^{5k}-CA_8 nanoparticles biodistribution after i.v. injection in subcutaneous SKOV3-luc tumor bearing mice. (A) *In vivo* optical images of real-time tumor targeting characteristics of PEG^{5k}-CA_8 nanoparticles. The location and possible metastasis of SKOV3-luc tumor was determined with bioluminescence by injecting i.p. 150 mg/kg luciferin. Tumor bearing mice were injected i.v. with the equivalent amount of free DiD dye or DiD-PTX-NPs. The optical imaging was obtained using Kodak multimodal imaging system IS2000MM equipped with an excitation bandpass filter at 625 nm and an emission at 700 nm. (B) Representative *ex vivo* optical images of tumors and organs of SKOV3-luc bearing mice sacrificed at 72h. (C) Time-dependent tumor accumulation profile of DiD-PTX-NPs. It

was semi-quantified as the tumor/background (normal skin) ratio of fluorenscence intensity (n=3). (D) quantitative fluorescence intensities of tumors and organs from *ex vivo* images (n=3). (E) Microscopic images of the tumor and normal muscle tissue. The nuclei were stained by DAPI (blue), and the signal of DiD (red) were acquired using Olympus FV1000 laser scanning confocal microscopy.

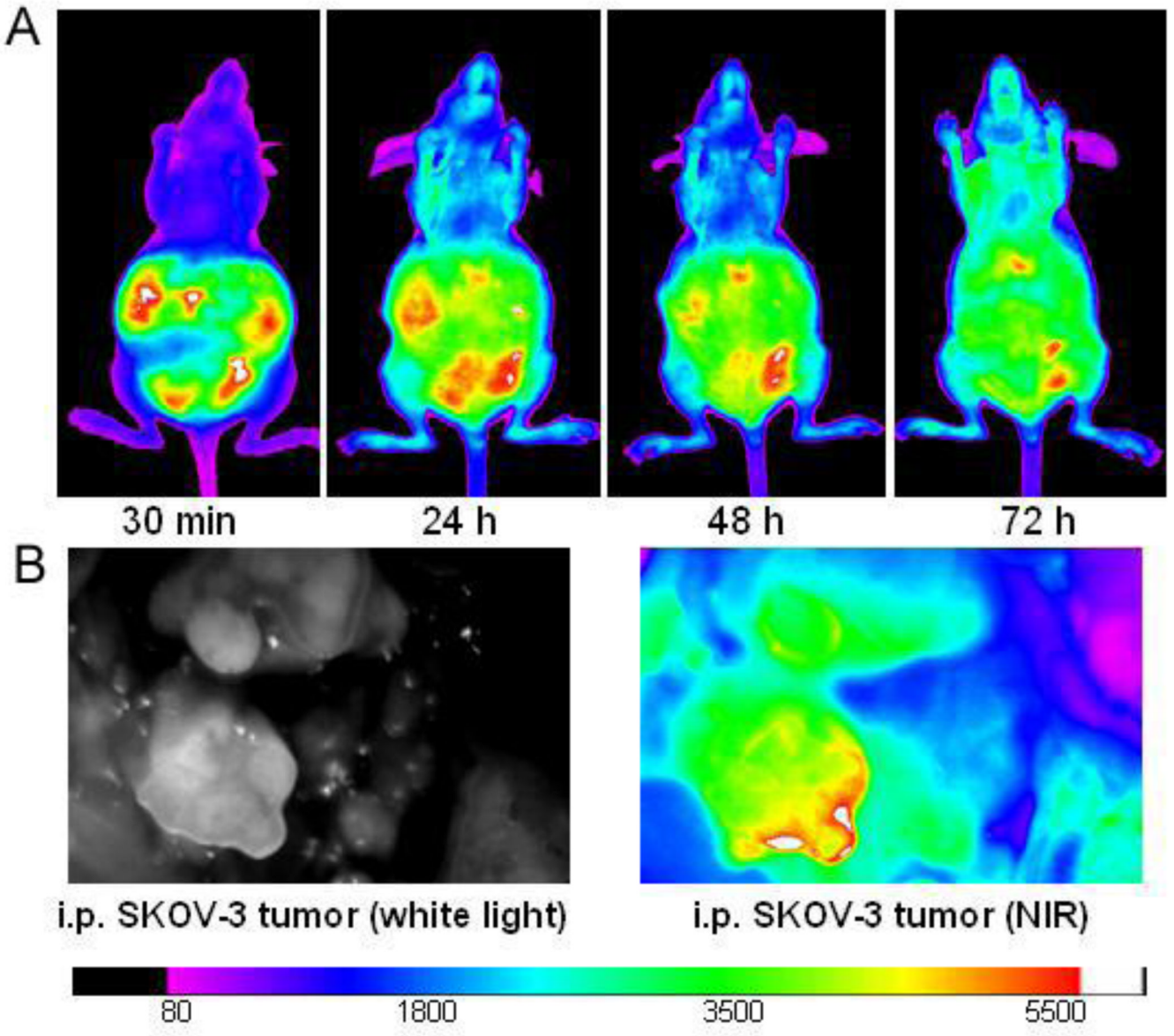

Fig. 6.

Intra-abdominal distribution of PEG^{5k}-CA_8 nanoparticles. (A) *In vivo* NIRF imaging of the intraperitoneal SKOV-3 tumor bearing mice at different time points after i.p. injection of DiD-PTX-NPs. (B) Localization of DiD-PTX-NPs on tumors. The mice were sacrificed at 72 h post injection, and the abdominal cavity was exposed to scan with Kodak imaging station.

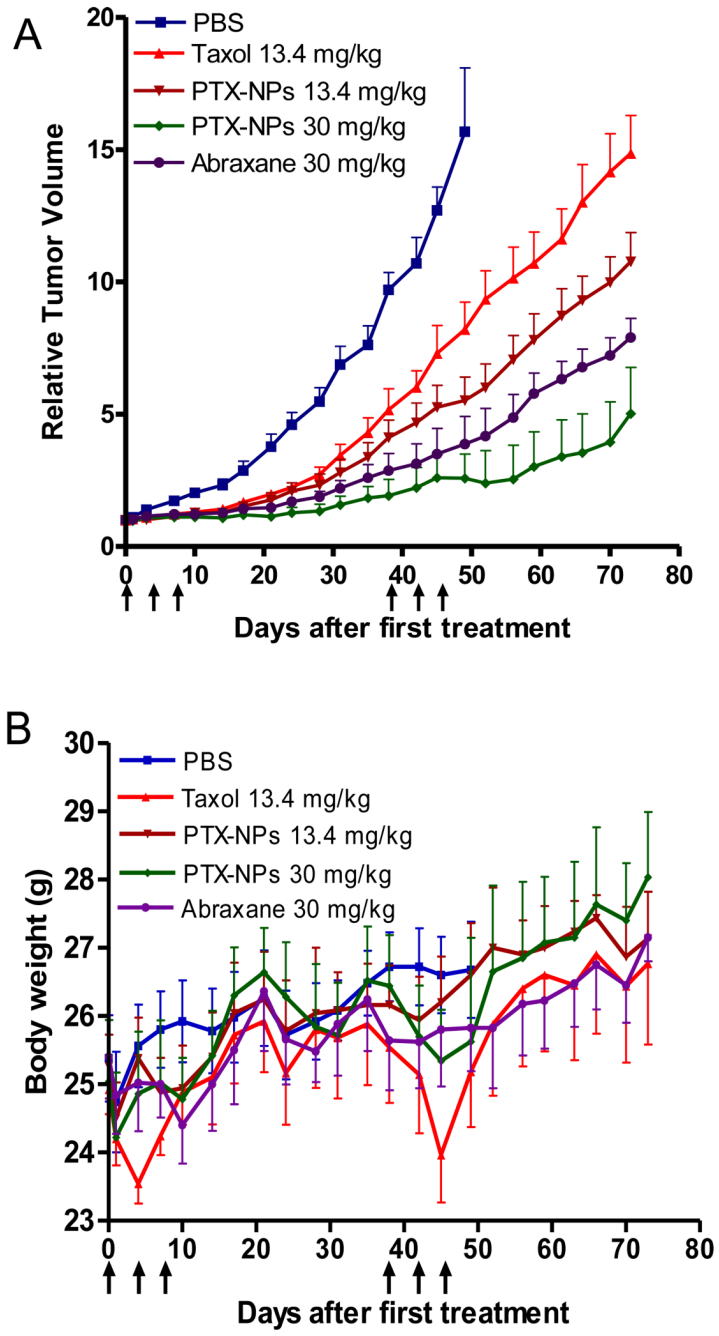

Fig. 7.

In vivo anti-tumor efficacy (A) and body weight changes (B) after intravenous treatment of different PTX formulations in the subcutaneous mouse model of SKOV3-luc ovarian cancer. Tumor bearing mice were administered i.v. with PBS (control), Taxol®, Abraxane® and PTX-PEG^{5k}-CA_8 NPs on days 0, 4, 8 and days 38, 42, 46 when tumor volume reached about 100~200 mm^3. Data represent mean ± SEM of six mice per group.

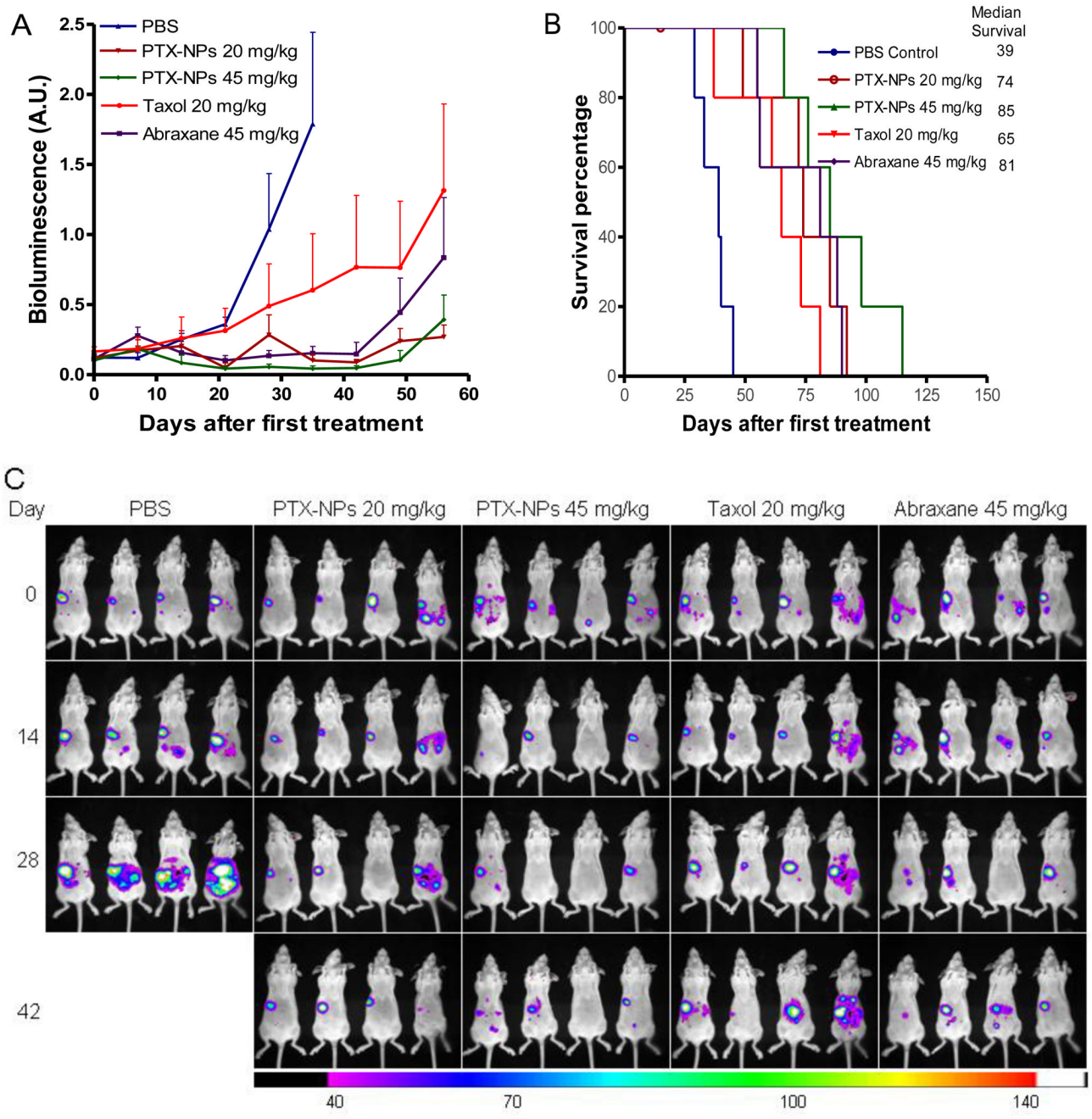

Fig. 8.

The anti-tumor efficacy after intraperitoneal therapy of different PTX formulations and noninvasive bioluminescence imaging in a murine model of peritoneally disseminated ovarian cancer. (A) Bioluminescence emitted by luciferase-expressing SKOV3-luc cancer cells at different time points after treatment. Peritoneal SKOV3-luc tumors bearing mice received total five intraperitoneal injection of Taxol®, Abraxane® and PTX-PEG^{5k}-CA$_8$ NPs on day 0, 4, 8, 12 and 16. Control groups received PBS only. Signal from the entire abdominal region of each mouse were quantified, and background was subtracted by measuring same sized ROIs in areas without light emission. (B) Survival of mice in different treatment groups. Open circle represents censored data point secondary to a death during anesthesia (i.e., not tumor-related).

(C) Representative pseudocolor images of intraperitoneal tumor burden. Color scale minimum and maximum have been adjusted so that they are identical in each image.